A Slotted-Patch Antenna Sensor With Higher Sensitivity for Detecting Setting Time of Cement Paste

Zhuoran Yi, Songtao Xue, Liyu Xie, *Member, IEEE*, Guochun Wan, *Member, IEEE*, and Chunfeng Wan

***Abstract*— A patch antenna can be applied to determine the setting time of cement paste by using resonant frequency as a sensing parameter to obtain real-time change of moisture content. However, for the traditional patch antenna sensor, the variation of its resonant frequency caused by moisture change is often interfered by environmental factors, especially the temperature effect. Based on the edge effect theory of the patch antenna, the extent of resonant frequency effects due to nearby material highly depends on the edge size of the radiation patch. To widen the variation range of the resonant frequency, we propose a slotted-patch antenna with multiple rectangular openings, which will consequently increase the edge area of a traditional patch antenna sensor. The proposed antenna sensor has enhanced sensitivity to the surrounding water ratio based on the electric flux theory and a numerical simulation by the Ansoft high-frequency structure simulator (Ansoft HFSS). The topological shape and dimension of the slotted-antenna sensor are determined numerically. The proposed sensor was fabricated and tested by wired interrogation. The results show that its variation ranges of resonant frequency increased 2.5 times over that of a rectangular patch antenna sensor. This improves the usability of a slotted patch antenna for detecting the setting time of cement paste.**

***Index Terms*— Cement hydration, setting time detection, slotted-patch antenna, testing range.**

I. Introduction

EVER since concrete was invented, it has remained one of the essential materials in civil engineering construction [1]. As a composite material, concrete is formed by cement, water, and aggregate, and the cement paste hardens and gains strength through a chemical reaction called hydration. Therefore, monitoring the cement hydration process helps ensure the safety of concrete structures during construction stages [2].

Previous work has already proposed several methods to detect the hydration state of cement, such as using a scanning electron microscope (SEM) [3] and X-rays [4]. These methods can provide detailed data for cement hydration. However, they always require the assistance of specific machinery, which is sometimes too cumbersome for practical use. When considering the condition of the construction site, it is better to obtain the most critical information rather than every tiny detail. Setting time is one of the most significant parameters for the monitoring of fresh cement paste during hydration. According to Chinese building code GB/T 1346-2011 [5], the setting time can predict the early-age strength and workability of cement. A construction project's timetable will be highly dependent on the setting time detection, and the structure may face failure due to cracks or low strength caused by an unqualified setting time [6].

For practical use, the setting time of cement is measured by the penetration resistance method specified in the European building code EN196-3-2016 [7]. In this method, the initial and final setting times are regarded as when the penetration resistance is achieved to a specific value. The speed and accuracy of this method are highly dependent on the experiments conducted by the construction workers. Besides, it is both time- and labor-consuming when the covered area of the structure is enormous.

To simplify the setting time testing period, several methods based on hydration temperature [8], ultrasonic velocity [9], [10], or impendence of inside copper sheets [11] were proposed. These methods do not need the laborers on site to repeat the penetration test. However, extra cables are necessary for practical use of the power supply and data transmission.

The initial setting time is defined as the time when the cement hydration reaches induction period, and the final setting time is defined as the time when the cement starts to obtain strength with the early hydration kind of finished [12], [13]. Since the cement hydration is defined as the reaction between water and cement, the hydration state can be reflected directly by the remained moisture inside the cement paste [9]. The main point of this method is to obtain the moisture content in a suitable way. Several methods detect the moisture content of concrete, such as magnetic resonance imaging [14] and time-domain reflectometry [15], [16]. Although these methods can obtain the moisture content accurately, each method needs

Manuscript received 24 May 2022; revised 4 July 2022; accepted 13 July 2022. Date of publication 29 July 2022; date of current version 15 August 2022. This work was supported in part by the National Natural Science Foundation of China under Grant 52078375 and Grant 52178298, and in part by the Top Discipline Plan of Shanghai Universities-Class I. The Associate Editor coordinating the review process was Dr. Shiraz Sohail. *(Corresponding author: Liyu Xie.)*

Zhuoran Yi and Liyu Xie are with the Department of Civil Engineering, Tongji University, Shanghai 200092, China (e-mail: yzr1997@tongji.edu.cn; liyuxie@tongji.edu.cn).

Songtao Xue is with the Department of Civil Engineering, Tongji University, Shanghai 200092, China, and also with the Department of Architecture, Tohoku Institute of Technology, Sendai 982-8577, Japan (e-mail: xue@tongji.edu.cn).

Guochun Wan is with the Department of Electronic Science and Technology, Tongji University, Shanghai 200092, China (e-mail: wanguochun@tongji.edu.cn).

Chunfeng Wan is with the Key Laboratory of Concrete and Prestressed Concrete Structure of the Ministry of Education, Southeast University, Nanjing 210096, China (e-mail: wan_seu@163.com).

Digital Object Identifier 10.1109/TIM.2022.3194853

samples and a power supply. Besides, to the best of our knowledge, a program designed to obtain cement setting time from its moisture content has not yet been invented. A more convenient way to test the moisture content and further detect the setting time is needed.

Since a patch antenna can be applied for moisture sensing [17], [18], it has shown feasibility in the application of setting time sensing. Teng *et al.* [19] proposed a moisture sensor for early-age cement paste based on a rectangular patch antenna. The return loss of the patch antenna is selected to reflect the moisture content of the surrounding cement paste. However, since the return loss of the patch antenna will always be affected by incident power, the interrogation distance must be kept nearly constant during the testing period, which is inconvenient for practical use. To overcome this shortcoming, Yi *et al.* [20] proposed a patch antenna-based setting time sensor, using the resonant frequency of the patch antenna to detect the moisture change and further obtain the setting time of surrounding cement paste. However, environmental and application issues, such as temperature effects, measuring, and fitting error, can also cause the operating resonant frequency shifting in the patch antenna sensor. Consequently, it will deteriorate the detection results of cement setting time. Hence, a patch antenna-based sensor with higher sensitivity to moisture change is more desirable for practical usage.

This article proposes an improved slotted-patch antenna sensor with multiple rectangular openings to enlarge the variation range of resonant frequency compared to traditional patch antenna sensors. The fundamental resonant frequency at the length direction is selected to reflect the effective dielectric constant, further show the moisture content of covering cement paste. Based on the equivalent theory of electric flux, the surrounding material will affect the resonant frequency of the surrounded patch antenna by changing the equivalent dielectric constant of the fringe substrate [21]–[24]. By increasing the fringe area of the patch antenna, the variation range of resonant frequency will increase. In this article, the slotted-patch antenna sensor utilizes several rectangular openings inside the radiation patch to enlarge the fringe area and ensure impedance matching at the same time. The antenna design can be more flexible in practical use, such as changing the shape with more edge or adding parasitic radiation patches.

This article is organized as follows. Section II introduces the sensing method of the patch antenna sensor for setting time detection. In Section III, a slotted-patch antenna sensor with rectangular openings is designed based on several previous slotted types and further optimized using Ansoft high-frequency structure simulator (Ansoft HFSS). In Section IV, the slotted-patch antenna sensor is fabricated. The typical patch antenna sensor and the slotted-patch antenna sensor are embedded inside the cement paste to compare the workability and verify the sensing performance. Conclusions are then drawn, and future research potential is discussed.

II. Sensing Method of Patch Antenna Sensor

A normal patch antenna sensor proposed in the previous work for the moisture content or setting time sensing is shown in Fig. 1, which consists of the radiation patch, substrate, and ground plane. The resonant frequency of the patch antenna sensor will change with a shift in the dielectric constant of the surrounding material. When a patch antenna sensor is embedded into cement paste, the dielectric constant of the nearby cement paste will approximately linearly decrease with the processing of cement hydration due to the decrease of moisture content, which further increases the resonant frequency of the patch antenna. Utilizing the theory proposed by Bernhard and Tousignant [24], Sun [25], Dirksen and Dasberg [26], Birchak *et al.* [27], and Perhirin and Auffret [28], the relationship between the resonant frequency of an embedded patch antenna sensor, moisture content, and the dielectric constant of surrounding cement paste is calculated and then displayed in Fig. 2. In this calculation example, the parameters being used are the same as those found in [20] and [29].

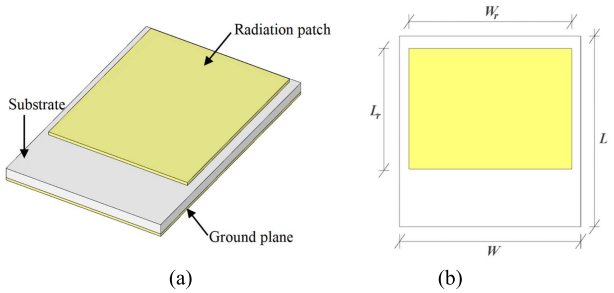

Fig. 1. Normal patch antenna sensor with (a) concept figure (b) top view.

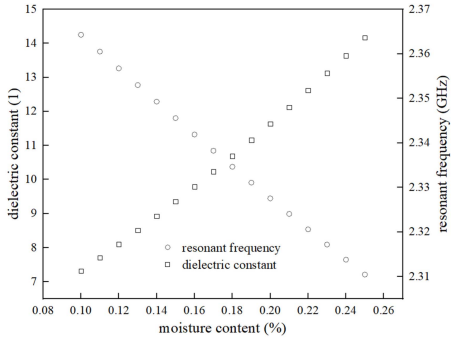

Fig. 2. Relationship between the resonant frequency of an embedded patch antenna, moisture content, and the dielectric constant of cement paste.

From Fig. 2, it is evident that the resonant frequency of a patch antenna will be affected by the moisture content of the covering material. Since the setting time is highly dependent on the moisture content of the cement paste, the patch antenna can be utilized for setting time sensing if the relationship is clear.

In this section, the working mechanism of the antenna sensor is illustrated. First, the relationship between moisture content, dielectric constant, and the resonant frequency is addressed. Then, the method to obtain the setting time of cement paste from the testing resonant frequency is investigated.

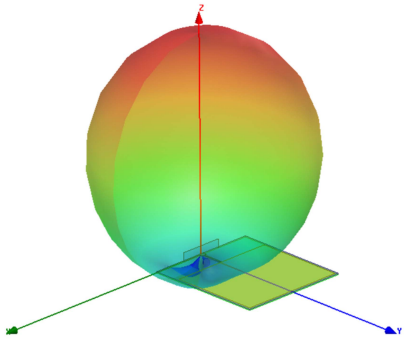

Fig. 3. Directivity of a normal patch antenna sensor.

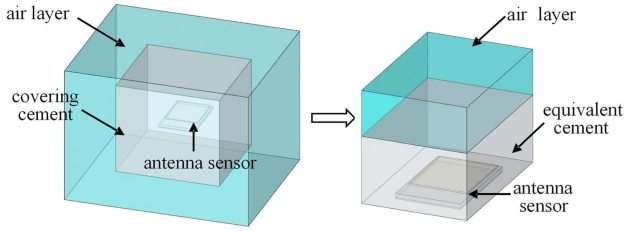

Fig. 4. Equivalent model of embedded patch antenna sensor.

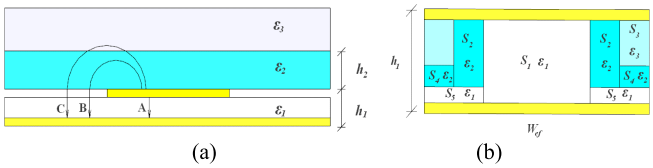

Fig. 5. Equivalent model using electric flux theory. (a) Electric flux path. (b) Equivalent patch antenna.

A. Measuring of the Change Tendency of Moisture

The directivity of a normal patch antenna sensor is shown in Fig. 3, using the parameter in Appendix A. Since the directivity of the patch antenna is in front of the radiation patch, the impact of the cement paste under the ground plane of the patch antenna sensor is ignored. Besides, the cement paste is regarded as a homogeneous material with a uniform dielectric constant for each hydration state. Based on these two assumptions, the working mode of the embedded patch antenna sensor can be equivalent to a dielectric-loaded patch antenna, as shown in Fig. 4.

Then, the effect of the surrounded cement paste can be expressed visually by the electric flux theory as Fig. 5(a). In this model, the dielectric constant of the substrate is ε_1. The embedded patch antenna sensor is covered by a cement paste layer with a dielectric constant of ε_2 and an infinite air layer with a dielectric constant of ε_3. The different paths of electric flux from the radiation patch to the ground plane represent the influence degree and location of covering material [21]. At the medium of the patch antenna sensor, the electric flux is mainly across the substrate as Path A. However, at the edge, the electric flux will cross the cement paste layer and the air layer as Paths B and C, which represents the effects of the covering cement paste, which is mainly concentrated at the edge of the radiation patch.

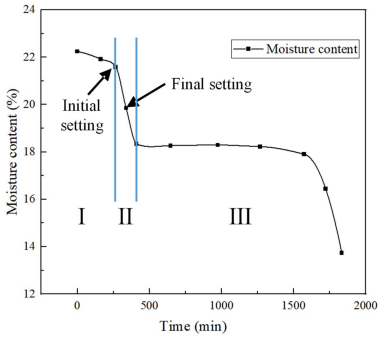

Fig. 6. Relationship between moisture content, hydration state, and setting time of cement paste [20].

Fig. 5(b) shows the equivalent model of the patch antenna sensor. In this model, Path A corresponds to the area S_1, while Paths B and C correspond to the area S_2–S_4. By choosing the longitudinal side as the resonant direction, the fundamental resonant frequency f_{tr} of the dielectric-loaded patch antenna can be represented as [30]

$$f_{\mathrm{tr}} = c\sqrt{(\pi/L_{\mathrm{r}})^2}/\left(2\pi\sqrt{\varepsilon_{\mathrm{e}}}\right) = c/\left(2L_{\mathrm{r}}\sqrt{\varepsilon_{\mathrm{e}}}\right) \tag{1}$$

where c is the light speed, L_{r} is the length of the radiation patch, and ε_{e} is the equivalent dielectric constant considering the effect of the covering material. The detailed relationship is shown in Appendix A [20], which has been analyzed in our previous work [21] and can be calculated as

$$\varepsilon_{\mathrm{e}} = F(\varepsilon_1, \varepsilon_2, \varepsilon_3, h_1, h_2, W_{\mathrm{r}}) \tag{2}$$

where h_1 and h_2 are the heights of the patch antenna sensor and covering cement paste, respectively, and W_{r} is the width of the radiation patch. From (1) and (2), the fundamental resonant frequency of the covered patch antenna sensor can be calculated theoretically if these basic parameters are known. In other words, this equation can be used in the optimization of the parameters. Besides, it is suitable to use the shift of resonant frequency to investigate the change tendency of the moisture in covering cement paste.

B. Setting Time Prediction

The setting time of cement paste is determined by the hydration state, which can be reflected by the change tendency of the cement's moisture. Taking Portland cement as an example, the relationship between the moisture content, hydration state, and setting time of cement paste can be explained through Fig. 6.

Stage I is the initial reaction period and induction period. In the initial reaction period, the fresh cement will react with the mixed water violently. During this period, the moisture will decrease rapidly but will only last briefly and come to the induction period soon. The cement hydration will nearly stop in the induction period, and the moisture content will keep nearly constant. After the induction period, the hydration will recover and result in a rapid decrease of moisture content,

called the acceleration period. This period will continue for about 1–4 h, followed by the after-acceleration period.

According to the early-age hydration stage, the initial setting will happen at the end of the induction period. The evaporation speed will keep nearly constant during the very early age [31]. To avoid the influence of evaporation, the change rate is selected to reflect the setting time. This moment can be recognized by detecting the inflection point of the moisture content (time with suddenly change in moisture content), which is expressed as

$$g(t) = f'(t) \tag{3}$$

where $g(t)$ is the change rate of moisture content and $f(t)$ is the moisture content.

The final setting time will approximately happen in the middle of the acceleration period. The final setting time is when the colloidal solids have bonded enough to form a calcium silicate hydrate (CSH) gel with basic strength. Since it will consume the majority of cement in the construction of CSH gel, the final setting time can be regarded as the time when the maximum speed of moisture decreases

$$g(t_{\text{fin}}) > g(t_{\text{fin}} \pm \Delta t)\Delta t \in R \tag{4}$$

where t_{fin} is the final setting time.

According to (3) and (4), the initial time and the final setting time can be predicted by investigating the change tendency of the moisture content, which can be obtained at the resonant frequency of the embedded patch antenna.

C. Environmental Effects

Since the resonant frequency will be influenced by the surrounding material and other environmental factors, such as temperature effect and environmental noise, the accuracy of setting time detection will decrease. Taking the temperature effect as an example, when the dielectric board is RT5880, the change occurred by the temperature effect is about 3%–7% of the change caused by the cement hydration according to Sanders *et al.* [32], Yao *et al.* [33], and Li and Wang [34]. Besides, the stress induced in the embedded concrete will also affect resonant frequency. In this part, the environmental effects are discussed quantitatively to show the advantage of the increased range of variations in resonant frequencies.

The environmental effect factors are analyzed first according to the cement setting. The main factors during the cement setting are temperature effect measuring and fitting error.

First considering the temperature effect. The maximum variation of temperature is set as 30 °C based on [35]. The temperature change will affect the resonant frequency by three aspects: influence the dielectric constant of cement paste, expanding the length of the radiation patch, and the dielectric constant of the dielectric board.

The effect of temperature to dielectric constant of cement paste is mainly determined by the influence to the dielectric constant of water. According to Owen's research [36], the dielectric constant of water will decrease from 80 to 70 when temperature increases from 20 °C to 50 °C, so it will introduce a maximum system error of about 12.5% to the sensor. This error cannot be reduced by expanding the variation range of resonant frequency.

TABLE I
BASIC PARAMETERS OF ANALYZING PATCH ANTENNA SENSOR

Parameters	L (mm)	W (mm)	L_r (mm)	h_1 (mm)	W_r(mm)
Value	54.3	51	41.3	0.508	49
Parameters	k_{t1} (ppm)	σ_t (kPa)	ε_e	k_{t2} (ppm)	ΔT_m (°C)
Value	40	150	2.2	−207	30

The expansion of patch length L_T mainly comes from two factors—the temperature stress of the patch antenna and the inner stress of cement during cement setting. The expansion can be calculated as follows, considering these two effects:

$$L_T = \left(k_{t1} L \Delta T - \sigma_t / E_{\text{p}}\right) \times L_{\text{r}} / L \tag{5}$$

where ΔT is the temperature range (with 20 °C set as the original temperature), and k_{t1} is the expanding coefficient of the dielectric board; thus, L and L_{r} are the original length of the patch antenna and the radiation patch, respectively; σ_t is the inner stress of embedded cement, which is set as 50% of the cracking strength, and E_{p} is the Young modulus of the patch antenna. Assuming that the dielectric board is made of Rogers RT5880 with one of the lowest dielectric constants in the market today, Young's modulus can be calculated as

$$E_{\text{p}} = 1046 - 8.05\Delta T. \tag{6}$$

The shift of the dielectric constant can also influence the resonant frequency. The variation of the dielectric constant ε_T caused by the temperature change, ΔT, is given as

$$\varepsilon_T = k_{t2}\varepsilon_{\text{e}}\Delta T \tag{7}$$

where ε_{e} is the original dielectric constant, and k_{t2} is the temperature coefficient of the dielectric constant.

Then, based on (1), (5), and (6), the resonant frequency variation Δf_T caused by temperature effect can be calculated by

$$\Delta f_T = f_T - f_{\text{o}} = \frac{c}{2(L_{\text{r}} + L_T)\sqrt{\varepsilon_{\text{e}} + \varepsilon_T}} - \frac{c}{2L_{\text{r}}\sqrt{\varepsilon_{\text{e}}}} \tag{8}$$

where f_{o} and f_T are the original resonant frequency and the resonant frequency considering temperature effect, respectively.

Similar resonant frequency variations are also discussed in [20], [37], and [38], and the parameters of the analyzing patch antenna are listed in Table I. After applying these parameters to (7), the relationship between the temperature and variations of resonant frequency is displayed in Fig. 7.

Fig. 7 shows that the resonant frequency variation Δf_T is about −3.69 MHz in an approximately linear tendency when the temperature change ΔT achieves 30 °C. Since the effect of moisture content remains nearly constant during the temperature change, it is set at 40 MHz according to [20]. The temperature effect is about 9.23% of the effect of moisture content.

Then, based on the previous experiment, the measuring and fitting error is about 1 MHz, and the error caused by the

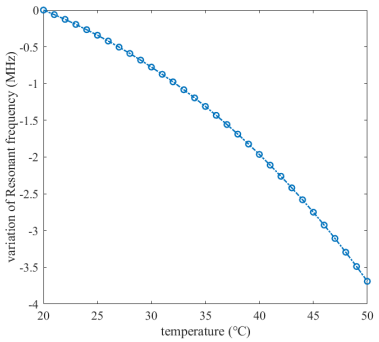

Fig. 7. Influence size of temperature effect.

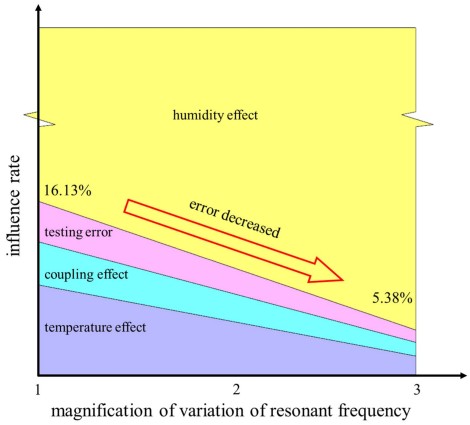

Fig. 8. Influence rate (side plot line) of several environmental effects with scale factor of variation in resonant frequencies (bottom plot line) [20].

coupling effect is about 3 MHz [20]. Taking all these effects into consideration, the composition of the resonant frequency variation during cement setting is displayed in Fig. 8.

From Fig. 8, the error caused by several environmental factors can be significantly decreased by increasing the influence rate of moisture content. That is, it is meaningful to propose a patch antenna sensor with a more extensive range of variations in resonant frequencies.

III. Proposal of Slotted-Patch Antenna Sensor

According to the electric flux model in Fig. 5, the surrounding cement paste mainly influenced the resonant frequencies of the embedded antenna through Paths B and C crossing the edge of the radiation patch. When the patch antenna is resonant on the length direction, the influence will mainly be dependent by the width of the radiation patch. From this aspect, if the length of the radiation patch keeps constant, increasing the aspect ratio of the radiation patch can enhance the effect of the cement paste covering and further enlarge the range of variations from the resonant frequencies.

Opening the slots on the radiation patch also provides a feasible entrance for this target. This section analyzes the effects of increasing the aspect ratio and opening slots in theory and in simulation. The basic parameters of the proposed patch antenna are also investigated in the theoretical analysis and are given in Table II.

TABLE II
Basic Parameters of Utilized Patch Antenna Sensor

Parameters	ε_1	ε_3	h_1 (mm)	L_r (mm)	μ_r	$tan\delta$
Value	2.2	1	0.508	41.3	0.99991	0

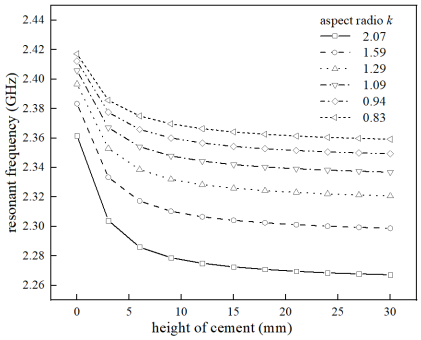

Fig. 9. Reflection of the aspect ratio with variations of covering height in theory.

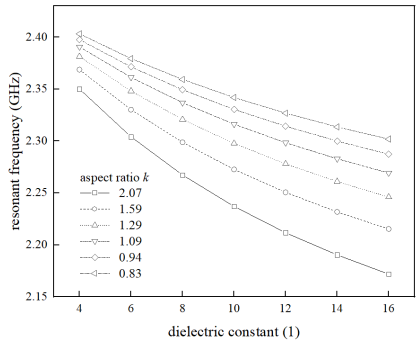

Fig. 10. Reflection of the aspect ratio with variations in dielectric constant in theory.

A. Increasing Aspect Ratio Effects

One of the easiest ways to enlarge the edge area is to decrease the size of the radiation patch. Since the length of the radiation patch is coupled with the fundamental resonant frequency of the embedded sensor, reducing the width is a feasible method.

The following discussion first analyzes the effects of the aspect ratio theoretically and then verifies that analysis by a simulated model established by using Ansys HFSS version 15.

By choosing the patch antenna sensor with parameters in Table II as a research item, the effect is analyzed using (1) in Section II-A. The relationship between the range of resonant frequencies, covering height h_2, dielectric constant ε_2, and aspect ratio k of the radiation patch is shown in Figs. 9 and 10.

μ_r and tan δ are the relative permeability and loss angle tangent of proposed cement paste, respectively.

Fig. 9 shows the reflection of the aspect ratio when the height of the covering cement paste h_2 increased from 0 (original patch antenna) to 30 mm (embedded patch antenna). During the height variation, the dielectric constant of cement paste ε_2 was set at 8 to simplify the calculation. During the

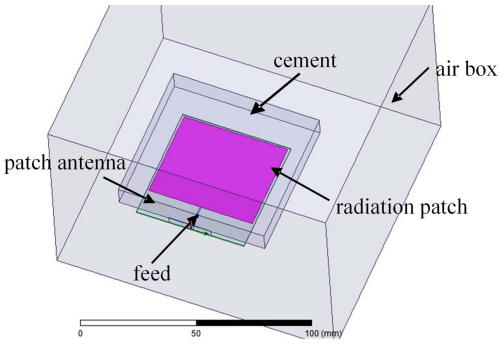

Fig. 11. Model showing the aspect ratio effects in Ansoft HFSS.

analysis, the resonant frequency of the patch antenna is decreased with the increase of the cement height. Besides, with the rise of the aspect ratio k (from 0.83 to 2.07), the variation of resonant frequency is increased from 0.05 to 0.09 GHz. The resonant frequency decreased rapidly at first and then converged to a constant. That is, the effect of the frequency change was to create a constant if the height of the covering cement was more than 30 mm.

Fig. 10 shows the reflection of the aspect ratio when the dielectric constant of the covering cement paste is increased from 4 (dry state) to 16 (wet state) [39], [40]. To simplify the calculation, the height of the cement paste cover is equal to 30 mm during the shift of the dielectric constant. During the calculation, the resonant frequencies of the patch antenna are decreased with the increase of variations in the dielectric constant. Besides, with the increase of the aspect ratio (from 0.83 to 2.07), the variation of resonant frequencies is increased from 0.10 to 0.18 GHz.

To further confirm the effect of the decreasing aspect ratio, the resonant frequency variations and the radiation efficiency were simulated in the Ansoft HFSS, version 15. Fig. 11 is the model established in Ansoft HFSS, which consists of a regular patch antenna and a covering dielectric block. The material of the dielectric board in the patch antenna is selected as Rogers RT/[1]duroid 5880. The radiation patch and ground plane are equivalent to a plane with the boundary of Perfect E to estimate the radiative properties of the metal conductor. According to the simulation, the width of the radiation patch will change while the length is staying constant. Since the cement is not a predefined material in Ansoft HFSS, the material covering the dielectric block is defined originally with a changeable dielectric constant shifting from 4 to 16 according to previous research. Both the patch antenna and the dielectric block are set inside an air box. The minimum length of the air box is set at more than a quarter wavelength to estimate the influence of the far-field radiation. The whole model is fed by a wave port at the end of the patch antenna.

For different aspect ratios, the height and dielectric constant of the covering dielectric block were often changed, and the resonant frequency of the covered patch antenna was analyzed. To keep the accuracy of comparison between the theoretical and simulation results, the basic setting of the patch antenna sensor is the same as the parameters utilized in Section II-B.

[1]Registered trademark.

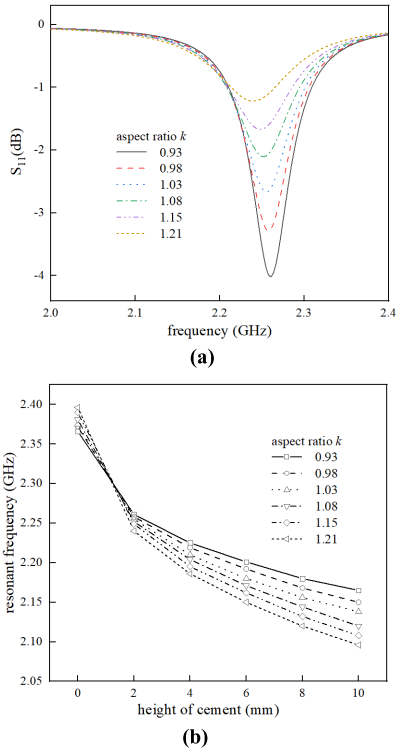

Fig. 12. Reflection of the aspect ratio with covering height variations in simulation. (a) Return loss curve (when h is consistently equal to 2 serving as a constant) and (b) effects of the aspect ratio.

Fig. 12 presents the effects of aspect ratio when the height is changed from 0 to 10 mm. First, the effect of the aspect ratio on the impendence match is analyzed and displayed in Fig. 10(a). According to the research, to simplify the calculation, the height of the cement is set at 2 mm. With the increase of the aspect ratio, $S11$ will decrease rapidly from -4 to -1 dB, which is not suitable for signal transmission.

Fig. 12(b) shows the influence of the aspect ratio on the variation of the resonant frequency. The dielectric constant of the covering dielectric block is set as 8 during simulation. Like the theoretical result, the resonant frequencies of the patch antenna will decrease with the expansion of cement height, and their variations will increase due to the increase of aspect ratio.

Fig. 13 presents the impact of the aspect ratio when the dielectric constant increased from 4 (dry state) to 16 (wet state). The height of the covering dielectric block is set at 30 mm during the simulation. Fig. 13(a) also declared that the impendence match will worsen with the increased aspect ratio. Fig. 13(b) indicates that the resonant frequency will decrease due to the ongoing increase of the dielectric constant. With the growth of aspect ratio, the variations in resonant frequency will expand from 0.132 to 0.234 GHz.

According to Figs. 9, 10, 12, and 13, it is evident that both the theoretical and simulated results show that the resonant frequency variations can be expanded by increasing the aspect ratio. However, the impedance will mismatch due to

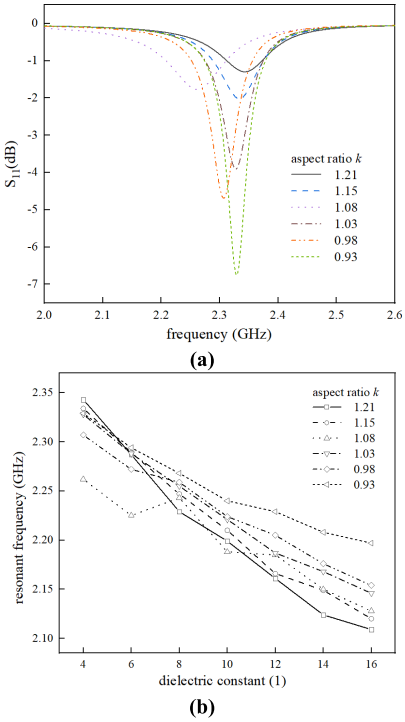

Fig. 13. Comparison of theoretical and simulated results when dielectric constant changes (a) return loss curve (when dielectric constant ε_2 is constantly equal to 4) and (b) influence of aspect ratio.

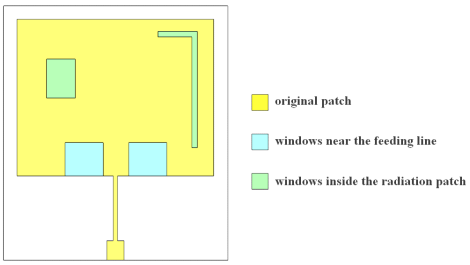

Fig. 14. Type of slots in the radiation patch.

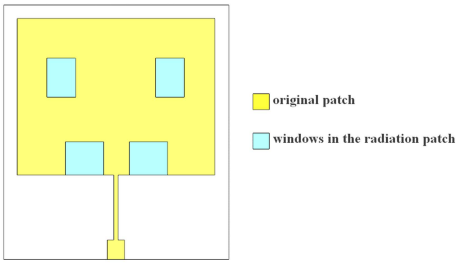

Fig. 15. Rectangular slots in the radiation patch designed by the authors for this research.

the increase in the aspect ratio, which should be considered carefully in further optimization efforts.

B. Effects of Opening Slots on the Radiation Patch

Based on the calculation above, it is obvious that the variation range of resonant frequencies can be enlarged by the increase in the aspect ratio. However, a low aspect ratio will cause an impedance mismatch [41], [42]. According to the research of Balanis [43], the most suitable aspect ratio k_s for a normal patch antenna sensor, as shown in Fig. 1, can be calculated as

$$k_s = L/W = \sqrt{2/[(\varepsilon_e + 1)\varepsilon]}. \tag{9}$$

When the aspect ratio is larger than k_s, the antenna radiation efficiency will decrease significantly due to the impedance mismatch. That is, the antenna sensor should be specifically designed to meet the basic requirement of radiation efficiency. Based on the research of Lamsalli *et al.* [44], the input resistance can be adjusted by opening slots on the radiation patch. Since the impedance match is mainly dependent on the input resistance, the radiation efficiency of the patch antenna sensor can be optimized by changing the location of the openings. Since the extra slots in the patch will increase the edge area, they can also be utilized to enlarge the variation range of the resonant frequencies.

Before the analysis, the basic type and location of the slots should be verified. When opening a window on the radiation patch, the current distribution will change, further affecting the resonant frequency and input impedance. The window on the radiation patch can be classified roughly by location: one is near the feeding line, and the other is inside the radiation patch, as shown in Fig. 14.

On the one hand, according to the Balanis survey [43], the feeding line will introduce extra capacitance to the patch antenna, which will decrease the input impedance and further influence the impedance matching. Opening slots near the feeding line can introduce extra inductance to prevent the effect of the feeding line, so two slots near the feeding line are necessary. On the other hand, several slots should be opened on the radiation patch to increase the edge area of the patch antenna. For a regular rectangular patch antenna, the most common shapes of slots opened on a radiation patch are L shaped [45], [46], U shaped [47], rectangular [48], and circular [49]. To simplify the calculation, the selected shape of slots inside the radiation patch for this experiment was rectangular; thus, two sets of symmetrical rectangles are displayed in Fig. 15.

While the basic shape of the patch antenna is determined, the optimized parameters of the sensors can be analyzed. Since the effects of the slots cannot be estimated theoretically, HFSS 15 was utilized to verify the effect of opening slots on the radiation patch and further determine the basic parameters of the slotted-patch antenna sensor with rectangular openings.

C. Design of the Slotted-Patch Antenna Sensor

Based on the analysis of the influence of the decreasing inspect ratio and opening slots on the radiation patch, the concept figure of the sensor design using a slotted-patch antenna is displayed in Fig. 16. First of all, the aspect ratio was minimized to increase the edge area. Then, four slots were opened on a thinner radiation patch with the basic shape and location. The suitable size and location of the slots were discussed after that.

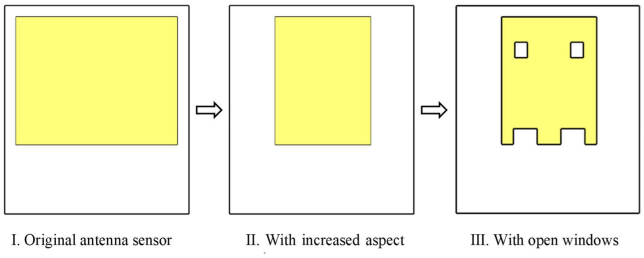

Fig. 16. Optimized step.

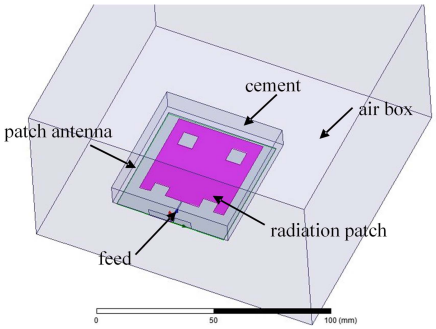

Fig. 17. Model showing the influence of opening slots in Ansoft HFSS.

TABLE III
OPTIMIZED PARAMETERS OF SLOTTED-PATCH ANTENNA SENSOR

Parameters(mm)	W_{r2}	L_{r2}	a	b	c	d
Value	29	36	1.5	3	9.4	5.5

The resonant frequency variation and the radiation efficiency are simulated in the Ansoft HFSS software program, version 15. Fig. 17 is the model established in Ansoft HFSS, which consists of a slotted-patch antenna with rectangular openings and a covering dielectric block. Like the model shown before, the material of the dielectric board in the patch antenna was selected as Rogers RT/duroid 5880. According to the simulation, the location and area of the slots in the radiation patch will change. To compare with the normal patch antenna sensor analyzed before, the material in the covering dielectric block was originally described as having a changeable dielectric constant shifting from 4 to 16 according to previous research. Both the patch antenna and the covering dielectric block are set inside an air box.

The location and area of the four slots on the radiation patch are then optimized through ergodic study. The location of the slots is controlled by parameters a and b, and the area of the slots is specified by the length of the window sides c and d. Other concerned parameters, including the width W_{r2} and length L_{r2} of the radiation patch, are also considered in this section.

To increase the impendence match, the final optimized parameters are shown in Fig. 18 and Table III. The final results corresponding to these parameters are shown in Fig. 19. Compared to the original type (−8 dB) and the no-opening type (−4 dB), the return loss at the radiation frequency is

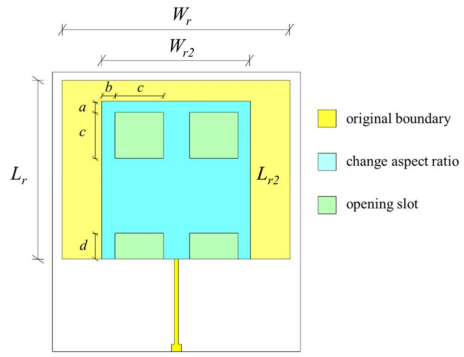

Fig. 18. Optimized shape of slotted-patch antenna sensor.

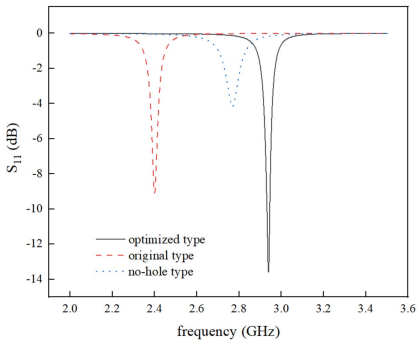

Fig. 19. Return loss curve for the optimized patch antenna sensor.

lower than −14 dB, which indicates that the impedance match is much better than the normal patch antenna sensor.

Then, the slotted-patch antenna was selected to test the sensitivity of the covering material. The process design is similar to the workflow carried in Section III-A. At first, the height of the material is increased from 0 to 30 mm, while the dielectric constant of the covered material remains as a constant as 8. After that, the dielectric constant of covering material shifts from 4 to 16, with the height staying constant at 30 mm. The results are presented in Fig. 20.

From Fig. 20(a), it is clear that the effect of height for all three types is converged to a constant when the height is high enough, which is similar to the phenomenon presented in the theoretical part. Besides, both Fig. 20(a) and (b) indicates that the variation range of the resonant frequency can be increased by decreasing aspect ratio and opening slots on the radiation patch.

Table IV compares three types or resonant frequency from exact data. The variation range of resonant frequency can be enlarged about three times by opening slots and comparing the results to the original status. Since the workability was affected by the testing condition, the original patch antenna and slotted-patch antenna were fabricated based on the parameters in Tables I–III. They were tested in the lab to further confirm the performance of the optimized patch antenna sensor.

IV. EXPERIMENT

The experiment is designed to verify the availability of the proposed sensors. The original patch antenna sensor is

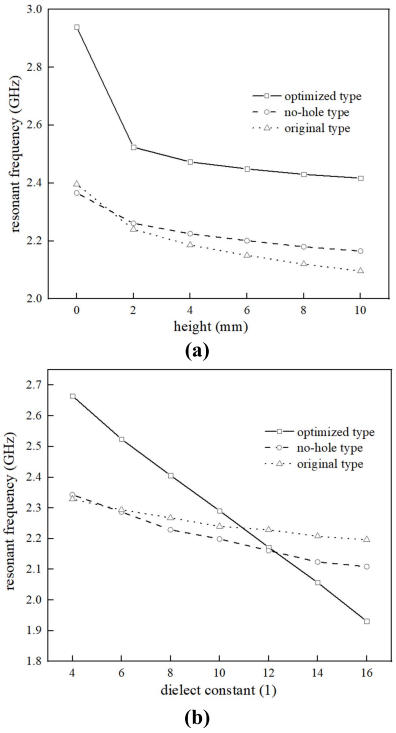

Fig. 20. Effects of (a) height and (b) dielectric constant.

TABLE IV
COMPARISON OF SIMULATED RESULTS FROM THREE STATES OF RESONANT FREQUENCIES

Parameters (GHz)	Start frequency		Start frequency		Variation range	
	h_2	ε_2	h_2	ε_2	h_2	ε_2
Slotted-patch	2.939	2.665	2.417	1.931	0.522	0.734
Width-reduced patch	2.396	2.343	2.096	2.109	0.300	0.234
Original patch	2.366	2.329	2.165	2.197	0.201	0.132

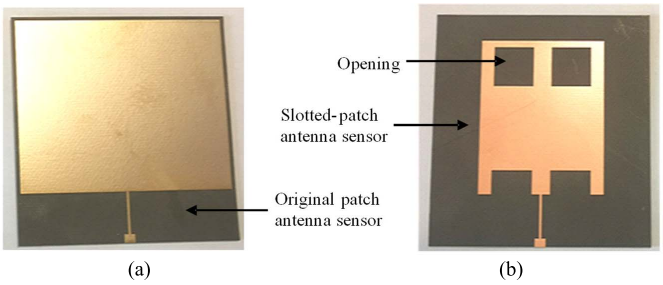

Fig. 21. Fabricated patch antenna sensors. (a) Original patch antenna sensor. (b) Slotted-patch antenna sensor.

fabricated as a control group based on the parameters in Table II, and the optimized patch antenna sensor was set in the experimental group based on the parameters in Table III. We replicated the simulation setting in Section III by utilizing both the original type and optimized type of RT/Duroid 5880 with copper as the material. The products are shown in Fig. 21.

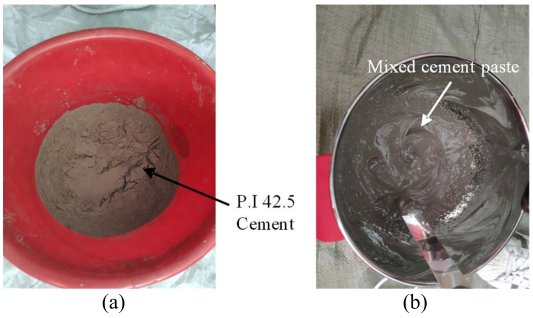

Fig. 22. Utilized cement paste. (a) P.I 42.5 cement. (b) Mixed cement paste.

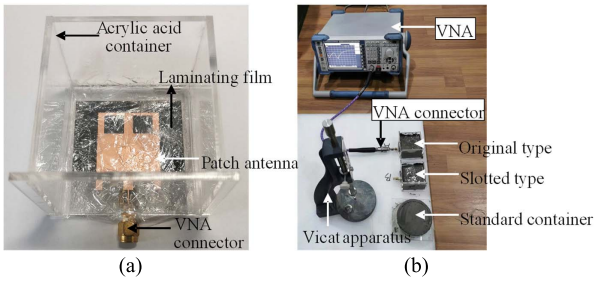

Fig. 23. Experimental setup. (a) Package design of antenna sensor and (b) testing setup of Vicat apparatus with VNA and three types of containers—original, slotted, and standard.

We chose P.I 42.5 Portland cement to make the cement paste for the setting time detection, as shown in Fig. 22. The temperature and humidity of the experiment room are keep as 20 °C and 50% according to the experiment.

A. Testing Method

The return loss curve of two antenna sensors was obtained from a vector network analyzer (VNA) through the coaxial line every 10 min. Each test was repeated three times to ensure testing accuracy. The resonant frequency has the lowest return loss in the average return loss curve. Therefore, the resonant frequency was utilized to calculate the initial setting time and final setting time of the cement paste.

B. Instrumentation Setup and Group Arrangement

The exact setting time result was measured using a Vicat apparatus to test the cement from the same batch [5]. A thin testing needle was utilized to stick the cement paste in a standard container every 10 min. According to the standard container dimensions, the cement paste will achieve the initial setting when the penetrated depth is lower than 67 mm. As soon as the cement paste reaches the initial setting, the container will be turned over, and a thicker needle will then poke the bottom surface of the paste. The final setting time is regarded as the time when the needle cannot leave scars on the surface of the paste.

The experiment was established, as shown in Fig. 23. First of all, two types of patch antenna sensors were placed inside an acrylic acid container. The surface of each sensor was covered by a thin laminating film for waterproofing. At the end of

TABLE V
PARAMETERS FOR TWO GROUPS

Parameter	Group A	Group B
Maximum height of cement paste (mm)	30	
Dimension of container (mm^3)	$52\times73\times66$	
Embedded patch antenna type	original	slotted

TABLE VI
DISTINCT DEGREE OF THE SCAR

Time (min)	245	275	305	310	315	320
Degree	Clear	Clear	Only half	Only half	Only half	Unable to recognize

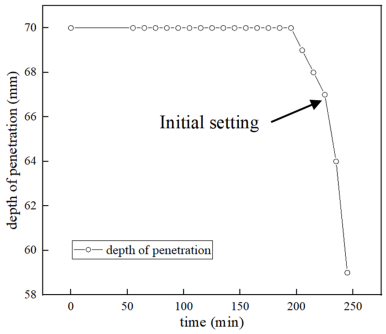

Fig. 24. Relationship between time and depth of penetration.

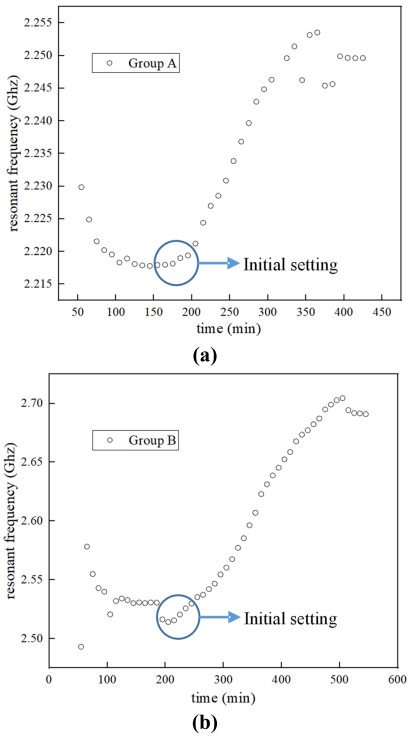

Fig. 25. Relationship between time and fundamental resonant frequency. (a) Group A. (b) Group B.

the patch antenna sensor, an subminiature version A (SMA) connector was soldered. Then, the mixed cement paste was injected into the two containers (the original container and the slotted container) and one standard container. A VNA and a Vicat apparatus were utilized to interrogate resonant frequency and setting time, as shown in Fig. 23(b).

As shown in Fig. 23, two groups are designed, and the parameters are listed in Table V. The basic material and size are the same for the two containers. Group A contains the original patch antenna sensor, while the slotted-patch antenna sensor is embedded in Group B. According to the research presented in Sections II and III, the height of cement paste was designed equally to 30 mm to consider the influence of cement paste fully.

C. Result and Discussion

The setting time obtained from both the patch antenna sensor and Vicat apparatus is calculated in this section first. Then, the variation range of resonant frequencies for the two antenna sensors is compared.

The penetrated depth of the Vicat apparatus as a function of time is displayed in Fig. 24, and the distinct degree of the needle-caused scar is shown in Table VI. According to Chinese standard GBT 1346-2011 [5], the initial setting time is 225 min, and the final setting time is 320 min.

The fundamental resonant frequencies of the two patch antenna sensors were then analyzed and are shown in Fig. 25. For both groups, the shapes of resonant frequencies are similar to an inverted Z, which relates to the relationship between the moisture content and time. The change tendency of the resonant frequency can be utilized to show the changing tendency of moisture content.

According to the results in Section II, the initial setting time of cement paste can be obtained from the time when the resonant frequency rates (moisture content) start to increase rapidly. As circled in Fig. 25, the initial setting time is 195 min for Group A and 215 min for Group B. Each point of resonant frequency has been test three times, and the resonant frequencies obtained from three $S11$ curves in the meantime have a difference about 1–2 MHz.

According to the results in Section II, the final setting time can be regarded as the time when the change rate of moisture content (resonant frequency) starts to decrease compared to the maximum data. To find the starting point, the change rate of the resonant frequency is calculated.

During the calculation, a moving window from point $n-m$ to point $n\ -m$ is set for each point n at time t. Then, the $2m+1$ continuous points are utilized for the linear fitting, and the slope of the fitted line is selected as the change rate of the resonant frequency at point n. In this article, the length of the moving window is selected as 7 (could also be 5, 9, or 11 and the results are similar). The final results are shown in Fig. 26.

According to the data in Fig. 26, the final setting time can be obtained in the circled area, which is 275 min for Group A and 355 min for Group B. The values of the two kinds of sensors are further listed and compared in Table VII. In this table, the relative sensitivity, S, of the two patch antenna sensors is defined as

$$S = \Delta f / f_{\text{basic}} = 2\Delta f / \left(f_{\text{up}} + f_{\text{be}}\right) \tag{10}$$

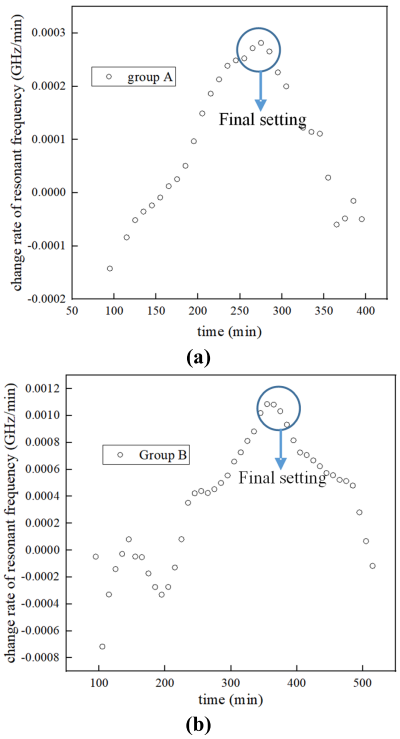

Fig. 26. Relationship between time and the changing rates of resonant frequencies. (a) Group A. (b) Group B.

TABLE VII
COMPARISON OF TWO EXPERIMENTAL GROUPS

Parameter	Vicat	Group A	Group B	Average
Initial setting time (min)	225	195	215	205
Error (%)	/	13.3	4.4	8.9
Final setting time (min)	320	275	355	315
Error (%)	/	14.1	10.9	1.6
Variation range (GHz)	/	**0.032**	**0.175**	/
Relative Sensitivity (1)	/	**0.0143**	**0.0671**	/

where Δf is the variation range of resonant frequencies, and f_{basic} is the working frequency, which is defined by Jeyaraj and Swaminathan [46] as

$$f_{\text{basic}} = \left(f_{\text{up}} + f_{\text{be}}\right)/2 \tag{11}$$

where f_{up} is the upper frequency and f_{be} is the lower frequency of the variation band.

Compared with the data obtained from Vicat, the error of the predicted setting time from both antenna sensors is lower than 15%, and the average error is lower than 10%, which indicates that the patch antenna sensor is useful for the setting time prediction. The error may be caused due to the difference between the two containers, which can be considered in the practical utilization.

The variation range of the resonant frequencies for Group B is over five times that of the range for Group A. Besides, the relative sensitivity is also increased nearly five times by using the slotted-patch antenna sensor. That is, by reducing the aspect ratio and opening slots on the radiation patch, the sensitivity of the antenna sensor can be increased rapidly, and the antenna sensor can achieve better workability.

V. CONCLUSION

This article introduces a slotted-patch antenna sensor utilized to detect the setting time of cement. The main purpose of this antenna sensor is to increase the influence of moisture content by enlarging the edge area, further avoiding the temperature effect and increasing the detection accuracy. An equivalent model based on the magnetic flux theory was used to verify the availability of the slotted-patch antenna sensor. Then, a parametric study was conducted through the simulated model in HFSS, version 15 to determine the size of the patch antenna sensor. The slotted-patch antenna sensor and a normal patch antenna sensor were then fabricated and tested in the lab. The error for setting time prediction based on the testing of the two sensors is lower than 15%, indicating that both sensors have a good workability in setting time detection. Besides, the variation range and relative sensitivity of the slotted-patch antenna sensor were increased approximately six and five times, respectively, compared to the original sensor. In other words, the slotted-patch antenna sensor can efficiently increase the variation range of resonant frequency and sensitivity when applied to detect the setting time of cement.

APPENDIX

This appendix shows a detailed way to calculate the resonant frequency of an embedded patch antenna. Consider the model in Fig. 5.

First, the antenna width will be enlarged due to the nonlinear flux path. The effective width W_{ef} of the equivalent patch antenna can be estimated as

$$W_{\text{ef}} = W + (2 \times h_1/\pi) \times \ln[17.08(w/2 \times h_1 + 0.92)]. \tag{A.1}$$

Then, the filling fractions q_1, q_2, and q_3 representing the capacitive effect of the three regions with different dielectric constants are expressed as follows:

$$q_1 = 1 - \frac{h_1}{2W_{\text{ef}}} \ln\left(\frac{\pi}{h_1} \times W_{\text{ef}} - 1\right) \tag{A.2}$$

$$q_2 = 1 - q_1 - \frac{h_1 - \upsilon_\varepsilon}{2W_{\text{ef}}} \times \ln\left[\left(\frac{\pi}{h_1} \times W_{\text{ef}} \frac{\cos\left(\frac{\pi \upsilon_\varepsilon}{2h_1}\right)}{\pi\left(\frac{h_2}{h_1} - \frac{1}{2}\right) + \frac{\pi \upsilon_\varepsilon}{2h_1}} + \sin\left(\frac{\pi \upsilon_\varepsilon}{2h_1}\right)\right)\right] \tag{A.3}$$

$$q_3 = \frac{h_1 - \upsilon_\varepsilon}{2W_{\text{ef}}} \times \ln\left[\left(\frac{\pi}{h_1} \times W_{\text{ef}} \frac{\cos\left(\frac{\pi \upsilon_\varepsilon}{2h_1}\right)}{\pi\left(\frac{h_2}{h_1} - \frac{1}{2}\right) + \frac{\pi \upsilon_\varepsilon}{2h_1}} + \sin\left(\frac{\pi \upsilon_\varepsilon}{2h_1}\right)\right)\right] \tag{A.4}$$

$$\varepsilon_{\mathrm{e}} = \varepsilon_1 q_{1n} + \frac{\varepsilon_1(1-q_{1n})^2 \times \left[\varepsilon_2^2 q_{2n} q_3 + \varepsilon_2 \varepsilon_3 \left(q_{2n} q_4 + (q_3+q_4)^2\right)\right]}{\varepsilon_2^2 q_{2n} q_3 q_4 + \varepsilon_1(\varepsilon_2 q_3 + \varepsilon_3 q_4)(1-q_{1n}-q_4)^2 + \varepsilon_2 \varepsilon_3 q_4 \left[q_{2n} q_4 + (q_3+q_4)^2\right]} \tag{A.9}$$

where the quantity v_ε is given as

$$v_\varepsilon = \frac{2h_1}{\pi} \arctan\left[\frac{\pi}{\frac{\pi \times W_{\mathrm{ef}}}{2h_1} - 2}\left(\frac{h_2}{h_1} - 1\right)\right]. \tag{A.5}$$

Due to the ignorance of the filling fraction expressions in the ultimate limit state when there is no covering material, (A.1)–(A.5) overestimate the effect of the second layer dielectric board with a dielectric constant of ε_2. To rectify the error, a new filling fraction q_4 is proposed by the following equation:

$$q_4 = (h_1/2W_{\mathrm{ef}}) \times \ln(\pi/2 + h_1/2W_{\mathrm{ef}}). \tag{A.6}$$

Then, two filling fractions, q_1 and q_2, are modified as q_{1n} and q_{2n} as

$$q_{1n} = q_1 - q_4 \tag{A.7}$$

$$q_{2n} = 1 - q_{1n} - q_3 - 2q_4. \tag{A.8}$$

The effective dielectric constant ε_{e} of the covered antenna can be calculated as (A.9), shown at the top of the page.

Considering the effect of effective length extension, the adjusted effective dielectric constant $\varepsilon'_{\mathrm{e}}$ is rewritten as

$$\varepsilon'_{\mathrm{e}} = (2\varepsilon_{\mathrm{e}} - 1 + K)/(1+K) \tag{A.10}$$

where K is

$$K = \sqrt{W_{\mathrm{ef}}/(W_{\mathrm{ef}} + 10h_1)}. \tag{A.11}$$

Finally, the resonant frequency f of the equivalent patch antenna is obtained by

$$f = cn/\left(2L_{\mathrm{r}}\sqrt{\varepsilon'_{\mathrm{e}}}\right) \tag{A.12}$$

where c is the speed of light, and n is the order of resonant frequency.

REFERENCES

[1] H. Alwashali, D. Sen, K. Jin, and M. Maeda, "Experimental investigation of influences of several parameters on seismic capacity of masonry infilled reinforced concrete frame," *Eng. Struct.*, vol. 189, pp. 11–24, Jun. 2019.

[2] K. J. Bois, A. D. Benally, P. S. Nowak, and R. Zoughi, "Cure-state monitoring and water-to-cement ratio determination of fresh Portland cement-based materials using near-field microwave techniques," *IEEE Trans. Instrum. Meas.*, vol. 47, no. 3, pp. 628–637, Jun. 1998.

[3] X. Feng, E. J. Garboczi, D. P. Bentz, P. E. Stutzman, and T. O. Mason, "Estimation of the degree of hydration of blended cement pastes by a scanning electron microscope point-counting procedure," *Cement Concrete Res.*, vol. 34, no. 10, pp. 1787–1793, Oct. 2004.

[4] T. J. Chotard, M. P. Boncoeur-Martel, A. Smith, J. P. Dupuy, and C. Gault, "Application of X-ray computed tomography to characterise the early hydration of calcium aluminate cement," *Cement Concrete Compos.*, vol. 25, no. 1, pp. 145–152, Jan. 2003.

[5] *General Administration of Quality Supervision, Inspection and Quarantine (AQSIQ) and Standardization Administration (SAC) of the People's Republic of China. Chinese Building Code GB/T 1346–2011, Test Methods for Water Requirement of Normal Consistency, Setting Time and Soundness of the Portland Cement*. Accessed: Jul. 20, 2011. [Online]. Available: https://www.chinesestandard.net/PDF.aspx/GBT1346-2011

[6] I. Pane and W. Hansen, "Concrete hydration and mechanical properties under nonisothermal conditions," *Aci Mater. J.*, vol. 99, no. 6, pp. 534–542, 2002.

[7] *European Build Code, Methods of Testing Cement—Part 3: Determination of Setting Times and Soundness*, Standard EN 196–3–2016, 2016.

[8] D. Luo, Z. Ismail, and Z. Ibrahim, "Added advantages in using a fiber Bragg grating sensor in the determination of early age setting time for cement pastes," *Measurement*, vol. 46, no. 10, pp. 4313–4320, 2013.

[9] G. Trtnik, G. Turk, F. Kavčič, and V. B. Bosiljkov, "Possibilities of using the ultrasonic wave transmission method to estimate initial setting time of cement paste," *Cement Concrete Res.*, vol. 38, no. 11, pp. 1336–1342, Nov. 2008.

[10] I. Gabrijel, D. Mikulić, and B. Milovanović, "Application of ultrasonic measurements for determination of setting and hardening in cement paste," *J. Civil Eng. Archit.*, vol. 5, no. 3, pp. 278–283, Mar. 2011.

[11] K. J. Akram, A. Ahmed, and T. Islam, "Fringing field impedance sensor for hydration monitoring and setting time determination of concrete material," *IEEE Trans. Instrum. Meas.*, vol. 69, no. 5, pp. 2131–2138, May 2020.

[12] J. W. Bullard *et al.*, "Mechanisms of cement hydration," *Cement Concrete Res.*, vol. 41, no. 12, pp. 1208–1223, 2010.

[13] K. Scrivener, A. Ouzia, P. Juilland, and A. K. Mohamed, "Advances in understanding cement hydration mechanisms," *Cement Concrete Res.*, vol. 124, Oct. 2019, Art. no. 105823.

[14] S. D. Beyea *et al.*, "Magnetic resonance imaging and moisture content profiles of drying concrete," *Cement Concrete Res.*, vol. 28, no. 3, pp. 453–463, Mar. 1998.

[15] W. N. Herkelrath, S. P. Hamburg, and F. Murphy, "Automatic, real-time monitoring of soil moisture in a remote field area with time domain reflectometry," *Water Resour. Res.*, vol. 27, no. 5, pp. 857–864, May 1991.

[16] R. Černý, "Time-domain reflectometry method and its application for measuring moisture content in porous materials: A review," *Measurement*, vol. 42, no. 3, pp. 329–336, Apr. 2009.

[17] M. M. Ghretli, K. Khalid, I. V. Grozescu, M. H. Sahri, and Z. Abbas, "Dual-frequency microwave moisture sensor based on circular microstrip antenna," *IEEE Sensors J.*, vol. 7, no. 12, pp. 1749–1756, Dec. 2007.

[18] E. M. Cheng *et al.*, "Development of microstrip patch antenna sensing system for salinity and sugar detection in water," *Int. J. Mech. Mechatronics Eng.*, vol. 14, no. 5, pp. 31–36, 2014.

[19] K. Teng *et al.*, "Embedded smart antenna for non-destructive testing and evaluation (NDT&E) of moisture content and deterioration in concrete," *Sensors*, vol. 19, no. 3, p. 547, Jan. 2019.

[20] Z. Yi, S. Xue, L. Xie, and G. Wan, "Detection of setting time in cement hydration using patch antenna sensor," *Struct. Control Health Monitor.*, vol. 29, no. 1, p. e2855, Jan. 2022.

[21] Y. Li and N. Bowler, "Resonant frequency of a rectangular patch sensor covered with multilayered dielectric structures," *IEEE Trans. Antennas Propag.*, vol. 58, no. 6, pp. 1883–1889, Jun. 2010.

[22] R. R. Wakodkar, B. Gupta, and S. Chakraborty, "Variation of resonant frequency of a rectangular microstrip patch antenna due to accumulation of water over its surface," in *Proc. Int. Conf. Appl. Electromagnetism Student Innov. Competition Awards (AEMC)*, Aug. 2010, pp. 239–243.

[23] T. Fortaki, L. Djouane, F. Chebara, and A. Benghalia, "Radiation of a rectangular microstrip patch antenna covered with a dielectric layer," *Int. J. Electron.*, vol. 95, no. 9, pp. 989–998, Sep. 2008.

[24] J. T. Bernhard and C. J. Tousignant, "Resonant frequencies of rectangular microstrip antennas with flush and spaced dielectric superstrates," *IEEE Trans. Antennas Propag.*, vol. 47, no. 2, pp. 302–308, Feb. 1999.

[25] Z. J. Sun, "Estimating volume fraction of bound water in Portland cement concrete during hydration based on dielectric constant measurement," *Mag. Concrete Res.*, vol. 60, no. 3, pp. 205–210, Apr. 2008.

[26] C. Dirksen and S. Dasberg, "Improved calibration of time domain reflectometry soil water content measurements," *Soil Sci. Soc. Amer. J.*, vol. 57, no. 3, pp. 660–667, 1993.

[27] J. R. Birchak, C. G. Gardner, J. E. Hipp, and J. M. Victor, "High dielectric constant microwave probes for sensing soil moisture," *Proc. IEEE*, vol. 62, no. 1, pp. 93–98, Jan. 1974.

[28] A. Frederic, Q. Veronique, G. Mikael, P. Andre, and A. Yves, "A low-consumption electronic system developed for a 10 km long all-optical extension dedicated to sea floor observatories using power-over-fiber technology and SPI protocol," *Microw. Opt. Technol. Lett.*, vol. 55, no. 11, pp. 2562–2568, Nov. 2013.
[29] S. Xue, Z. Yi, L. Xie, G. Wan, and T. Ding, "A passive wireless crack sensor based on patch antenna with overlapping sub-patch," *Sensors*, vol. 19, no. 19, p. 4327, Oct. 2019.
[30] S. Xue, Z. Yi, L. Xie, and G. Wan, "Double-frequency passive deformation sensor based on two-layer patch antenna," *Smart Struct. Syst.*, vol. 27, no. 6, pp. 969–982, 2021.
[31] İ. B. Topçu and V. B. Elgün, "Influence of concrete properties on bleeding and evaporation," *Cement Concrete Res.*, vol. 34, no. 2, pp. 275–281, Feb. 2004.
[32] J. W. Sanders, J. Yao, and H. Huang, "Microstrip patch antenna temperature sensor," *IEEE Sensors J.*, vol. 15, no. 9, pp. 5312–5319, Sep. 2015.
[33] J. Yao, F. M. Tchafa, A. Jain, S. Tjuatja, and H. Huang, "Far-field interrogation of microstrip patch antenna for temperature sensing without electronics," *IEEE Sensors J.*, vol. 16, no. 19, pp. 7053–7060, Oct. 2016.
[34] D. Li and Y. Wang, "Thermally stable wireless patch antenna sensor for strain and crack sensing," *Sensors*, vol. 20, no. 14, p. 3835, Jul. 2020.
[35] M. Azenha, R. Faria, and D. Ferreira, "Identification of early-age concrete temperatures and strains: Monitoring and numerical simulation," *Cement Concrete Composites*, vol. 31, no. 6, pp. 369–378, Jul. 2009.
[36] B. B. Owen, R. C. Miller, C. E. Milner, and H. L. Cogan, "The dielectric constant of water as a function of temperature and pressure[1,2]," *J. Phys. Chem.*, vol. 65, no. 11, pp. 2065–2070, 1967.
[37] S. Xue, Z. Yi, L. Xie, and G. Wan, "Simulation and experiment for temperature effect of unstressed patch antenna sensor with overlapping sub-patch," *J. Harb. Engin. Univ.*, vol. 42, no. 10, pp. 1439–1445, Oct. 2021.
[38] (2016). *RT/Duroid 5870/5880 High Frequency Laminates Data Sheet*. [Online]. Available: https://www.rogerscorp.com/documents/606/acm/RT-duroid-5870-5880-Data-Sheet.pdf
[39] M. Jamil, M. K. Hassan, H. M. A. Al-Mattarneh, and M. F. M. Zain, "Concrete dielectric properties investigation using microwave nondestructive techniques," *Mater. Struct.*, vol. 46, nos. 1–2, pp. 77–87, 2013.
[40] W. Chen, P. Shen, and Z. Shui, "Determination of water content in fresh concrete mix based on relative dielectric constant measurement," *Construct. Building Mater.*, vol. 34, pp. 306–312, Sep. 2012.
[41] C.-H. K. Chin, Q. Xue, and H. Wong, "Broadband patch antenna with a folded plate pair as a differential feeding scheme," *IEEE Trans. Antennas Propag.*, vol. 55, no. 9, pp. 2461–2467, Sep. 2007.
[42] J. R. Ojha and M. Peters, *Patch Antennas and Microstrip Lines*. London, U.K.: IntechOpen, 2010.
[43] C. A. Balanis, *Antenna Theory: Analysis and Design*. Hoboken, NJ, USA: Wiley, 2015.
[44] M. Lamsalli, A. El Hamichi, M. Boussouis, N. A. Touhami, and T. Elhamadi, "Genetic algorithm optimization for microstrip patch antenna miniaturization," *Prog. Electromagn. Res.*, vol. 60, pp. 113–120, 2016.
[45] R. Kozak, K. Khorsand, T. Zarifi, K. Golovin, and M. H. Zarifi, "Patch antenna sensor for wireless ice and frost detection," *Sci. Rep.*, vol. 11, no. 1, pp. 1–11, Dec. 2021.
[46] J. P. G. Jeyaraj and A. Swaminathan, "Broadband RCS reduction in microstrip patch antenna using L-shape stepped polarization rotation reflective surface," *Int. J. RF Microw. Comput. Eng.*, vol. 28, no. 7, pp. 1–6, 2018.
[47] O. W. Ata, M. Salamin, and K. Abusabha, "Double U-slot rectangular patch antenna for multiband applications," *Comput. Electr. Eng.*, vol. 84, Jun. 2020, Art. no. 106608.
[48] A. Khidre, K. F. Lee, F. Yang, and A. Eisherbeni, "Wideband circularly polarized E-shaped patch antenna for wireless applications," *IEEE Antennas Propag. Mag.*, vol. 30, no. 3, pp. 995–1001, Jun. 2010.
[49] R. A. Panda, D. Mishra, and H. Panda, "Biconcave lens structured patch antenna with circular slot for Ku-band applications," in *Proc. 2nd Int. Conf. Micro-Electron. Electromagn. Telecommun. (ICMEET)*, Jan. 2017, pp. 73–83.

Zhuoran Yi received the B.S. and M.S. degrees in civil engineering from Tongji University, Shanghai, China, in 2018 and 2021, respectively.

His current research interests focus on the smart sensors for the structural health monitoring and frequency modulated continuous wave (FMCW)-based radio frequency identification (RFID) detection systems.

Songtao Xue received the B.S. degree in mechanics engineering from Tongji University, Shanghai, China, in 1985, and the M.S. and Ph.D. degrees in structural engineering from Tohoku University, Sendai, Japan, in 1989 and 1991, respectively.

From 1991, he was as an Assistant Professor with the Department of Architecture, Tohoku University, where he was promoted to an Associate Professor in 1995. In 1996, he joined Tongji University, where he is currently a Full Professor. In 2010, he joined the Department of Architecture, Tohoku Institute of Technology, Sendai, where he is currently the Director of the Department of Architecture. His research interests focus on structural health monitoring, seismic engineering, and structural vibration control.

Liyu Xie (Member, IEEE) received the B.S. and M.S. degrees in mechanics engineering from Tongji University, Shanghai, China, in 2000 and 2003, respectively, and the Ph.D. degree in system design engineering from Keio University, Tokyo, Japan, in 2009.

Since 2009, he has been with the College of Civil Engineering, Tongji University, where he is currently an Associate Professor. His current research focuses on smart sensors, structural health monitoring, and structural vibration control.

Guochun Wan (Member, IEEE) received the M.S. and Ph.D. degrees in transportation information engineering and control from Tongji University, Shanghai, China, in 2005, and 2011, respectively.

He became an Associate Professor with Tongji University in 2002. He joined the Department of Electronic Science and Technology, Tongji University, in 2006. His current research interests include signal and information processing, with an emphasis on error-correcting coding, VLSI architectures, RFID strain sensor, and system-on-chip (SoC) design for communications and coding theory applications.

Chunfeng Wan received the B.S. degree from the University of Electronic Science and Technology of China, Chengdu, China, in 1997, the M.S. degree from Tongji University, Shanghai, China, in 2001, and the Ph.D. degree in system design engineering from Keio University, Tokyo, Japan, in 2009.

Since 2009, he has been with the School of Civil Engineering, Southeast University, Nanjing, China, where he is currently an Associate Professor. His current research interests include structural health monitoring and smart maintenance for civil infrastructures.